

Article

Asymmetrical Gaussian Potential Effects on Strongly Coupled Magnetopolaron Properties in Triangular Confinement Potential Quantum Wells

Jun Ge ¹, Shuang Han ², Xiujuan Miao ², Yong Sun ^{2,*}  and Jinglin Xiao ^{2,*}¹ College of Physics and Electronic Information, Hulunbuir University, Hulunbuir 021008, China² Institute of Condensed Matter Physics, Inner Mongolia Minzu University, Tongliao 028043, China

* Correspondence: sy19851009@126.com or sunyong@imun.edu.cn (Y.S.); xiaojlin@126.com (J.X.)

Abstract: In this research, the existence of an asymmetrical Gaussian confinement potential (AGCP) along the quantum well (QW) growth direction and of a parabolic potential perpendicular to the polar coordinate direction were considered. The magnetic field and temperature properties of the longitudinal optical (LO)-phonon mean number, ground-state energy (GSE), ground-state binding energy (GSBE) and vibrational frequency (VF) of strongly coupled magnetopolarons in triangular confinement potential QWs (TCPQWs) were investigated according to the quantum statistical theory as well as the linear combination operator and unitary transformation methods. We obtained analytical expressions for the GSE, GSBE, VF and LO-phonon mean number as functions of the applied magnetic field, temperature, AGCP barrier height, AGCP range, polar coordinate system's polar angle and polar coordinate system's confinement strength. It was demonstrated by the calculated numerical results that the GSE, GSBE, VF and LO-phonon mean number varied with the related physical quantities. The obtained theoretical results are expected to provide a reference for future research on polarons.

Keywords: vibrational frequency; temperature; magnetopolaron; LO-phonon mean number; ground-state binding energy; ground-state energy



Citation: Ge, J.; Han, S.; Miao, X.; Sun, Y.; Xiao, J. Asymmetrical Gaussian Potential Effects on Strongly Coupled Magnetopolaron Properties in Triangular Confinement Potential Quantum Wells. *Coatings* **2022**, *12*, 1900. <https://doi.org/10.3390/coatings12121900>

Academic Editor:
Tadeusz Hryniewicz

Received: 8 October 2022

Accepted: 1 December 2022

Published: 5 December 2022

Publisher's Note: MDPI stays neutral with regard to jurisdictional claims in published maps and institutional affiliations.



Copyright: © 2022 by the authors. Licensee MDPI, Basel, Switzerland. This article is an open access article distributed under the terms and conditions of the Creative Commons Attribution (CC BY) license (<https://creativecommons.org/licenses/by/4.0/>).

1. Introduction

Quasiparticles [1], also known as collective excitations, are sudden changes that occur in microcomplex systems. As an early quasiparticle–polaron concept, a polaron [2,3] was used to define the formation unit of excess carriers (electrons and holes) in potential wells generated by replacing the surrounding ions with carriers. In magnetic semiconductors, the carrier spin and surrounding magnetization cloud induced by them could be regarded as the quasicomposite particles called magnetopolarons. Theoretical and experimental research has described the importance of polarons in different systems [4–14]. It is worth mentioning that quantum well (QW) systems can be constructed with ionic crystals or polar semiconductor materials [15,16], therefore strongly affecting the physical properties [17–19] of electron–phonon interactions. Particularly, the photoelectric properties of different QW systems with peculiar quantum size effects have attracted the attention of some scholars to polarons [20–24]. Scientific and technological progress has introduced several external factors into the research field of QWs, such as magnetic fields [25,26], electric fields [27], pressure [28–30], confined potentials [31,32], etc., which have broadened the research field of QWs. When a polaron moves in a QW system, it interacts with the lattice and is influenced by different confined potentials. Confined potentials can be divided into strong and nonstrong confined potentials. For confined potentials, many studies have been conducted on the influences of different confined potentials on polaron properties. For example, Fotue et al. [33] calculated the time evolution of the quantum mechanical state of abundant magnetopolarons in a modified cylindrical quantum dot. In the condition of

strong coupling, they investigated the eigenenergies and eigenfunctions of the ground state and first excited state, respectively. Flebus et al. [34] theoretically studied the effects of strong magnetoelastic coupling on the transport properties of magnetic insulators. Kikkawa et al. [35] demonstrated that the sharp structures in the magnetic-field-dependent spin Seebeck effect voltages of Pt/Y₃Fe₅O₁₂ at low temperatures are attributed to the magnon–phonon interaction. Experimental results were well reproduced by the Boltzmann theory when it included magnetoelastic coupling. Li et al. [36] reported an observation of antiferromagnetic magnon polarons in a uniaxial antiferromagnetic insulator Cr₂O₃. By tracking the temperature dependence of the spin Seebeck effect anomalies, they found that magnon polarons showed behaviors similar to those of longitudinal acoustic and transverse acoustic phonons.

The importance of polarons in a variety of systems has been confirmed by several breakthroughs in experimental and theoretical studies. For example, in previous studies, polarons were influenced by parabolic potentials and asymmetric Gaussian potentials [37], or by parabolic potentials and asymmetric semi-exponential potentials [38], which led to a series of interesting phenomena. In order to further explore polaron-related problems, this paper discussed strongly coupled magnetopolaron properties in TCPQWs based on unitary transformation, the linear-combination operator method, and the quantum statistical theory. With continuous theoretical progress and the rapid accumulation of experimental evidence, it is hoped that the obtained results will contribute to research on the polaron effects in materials and other systems.

2. Theoretical Model

An electron was assumed to be in a 2D RbCl asymmetrical Gaussian confinement potential. The electron was considered to move in the crystal, interacting with bulk LO phonons. Magnetic field B was assumed to be along the z direction, $B = (0, 0, B)$, and was stated to have a vector potential in the Landau gauge, $A = B(-\frac{y}{2}, \frac{x}{2}, 0)$. Within the framework of the effective-mass approximation, we divided it into the electron energy, phonon energy and electron–phonon interaction energy and applied two limited potentials to it. Additionally, the electron–phonon Hamiltonian system in a triangular confinement potential QW (TCPQW) [39–41] was given by:

$$H = \frac{1}{2m} \left(p_x - \frac{\beta^2}{4} y \right)^2 + \frac{1}{2m} \left(p_y + \frac{\beta^2}{4} x \right)^2 + \frac{p_z^2}{2m} + \sum_{\mathbf{q}} \hbar \omega_{\text{LO}} a_{\mathbf{q}}^\dagger a_{\mathbf{q}} + \sum_{\mathbf{q}} (V_{\mathbf{q}} a_{\mathbf{q}} \exp(i\mathbf{q} \cdot \mathbf{r}) + \text{h.c.}) + V(z) + V_{\rho\theta}, \quad (1)$$

where

$$V(z) = \begin{cases} -V_0 e^{-\frac{z^2}{2R^2}} & z \geq 0 \\ \infty & z < 0 \end{cases} \quad (2)$$

$$V_{\rho\theta} = \frac{1}{2} m \omega_0^2 \rho^2 \left(1 + \frac{2}{7} \cos 3\theta \right) \quad (3)$$

where p is the electron momentum operator, m is the effective band mass, $\beta^2 = \frac{2eB}{c}$, $a_{\mathbf{q}}^\dagger$ and $a_{\mathbf{q}}$ are the creation and annihilation operators of the bulk LO phonon with frequency ω_{LO} and wave vector \mathbf{q} , $V(z)$ is the asymmetrical Gaussian confinement potential (AGCP), and $\mathbf{r} = (\rho, z)$ is the electron position vector. Additionally, z is the QW growth direction, V_0 is the asymmetrical Gaussian confinement potential barrier height, and R is the asymmetrical Gaussian confinement potential range. $V_{\rho\theta} = \frac{1}{2} m \omega_0^2 \rho^2 (1 + \frac{2}{7} \cos 3\theta)$ is the triangular

confinement potential, ρ is the polar coordinate system, θ is the polar coordinate system's polar angle, and ω_0 is the confinement strength. V_q and α in Equation (1) are defined as

$$\begin{aligned} V_q &= i(\hbar\omega_{LO}/q)(\hbar/2m\omega_{LO})^{1/4}(4\pi\alpha/V)^{1/2} \\ \alpha &= (e^2/2\hbar\omega_{LO})(2m\omega_{LO}/\hbar)^{1/2}(1/\epsilon_\infty - 1/\epsilon_0) \end{aligned} \tag{4}$$

A second Lee–Low–Pines (LLP) unitary transformation [42] on strong electron–phonon coupling gave:

$$U_2 = \exp\left[\sum_q (a_q^\dagger f_q - a_q f_q^*)\right] \tag{5}$$

in which $f_q(f_q^*)$ denotes the variational function. Then, linear combination operators [43] b_j^\dagger and b_j were introduced into Equation (1) as:

$$\begin{aligned} p_j &= (m\hbar\lambda/2)^{1/2}(b_j + b_j^\dagger) \\ r_j &= i(\hbar/2m\lambda)^{1/2}(b_j - b_j^\dagger) \end{aligned} \tag{6}$$

in which λ is the variational parameter and subscript j corresponds to the x , y and z directions. The ground-state wave function of the system was

$$|\psi_0\rangle = |0\rangle_a |0\rangle_b \tag{7}$$

where $|0\rangle_a$ and $|0\rangle_b$, which satisfied the $b_j|0\rangle_b = a_q|0\rangle_a = 0$ condition, denote the unperturbed zero phonon state and the vacuum state of the b operator, respectively. Then, the ground-state transformed Hamiltonian was anticipated to be $F(\lambda, f_q) = \langle \psi_0 | U_2^{-1} H U_2 | \psi_0 \rangle$. The conducting variations of $F(\lambda, f_q)$ were with respect to the variational function f_q and the vibrational parameter λ . The strongly coupled polaron vibrational frequency in a RbCl AGCP could be numerically derived as

$$\lambda^2 - \left(\frac{2\alpha}{3} \sqrt{\frac{\omega_{LO}}{\pi}}\right) \lambda^{\frac{3}{2}} - \left(\frac{V_0}{3mR^2} + \frac{4\omega_0^2}{3} \left(1 + \frac{2}{7} \cos 3\theta\right) + \frac{\omega_c^2}{6}\right) = 0 \tag{8}$$

Assuming the above equation's root to be λ_0 , the ground-state binding energy (GSBE) and the ground-state energy (GSE) of the polaron could be variationally derived as

$$E_0 = \frac{3}{4}\hbar\lambda - V_0 + \frac{\hbar V_0}{4m\lambda R^2} - \frac{1}{\sqrt{\pi}}\alpha\hbar\omega_{LO} \left(\frac{\lambda}{\omega_{LO}}\right)^{\frac{1}{2}} + \frac{\hbar\omega_c^2}{8\lambda} + \frac{\hbar\omega_0^2}{\lambda} \left(1 + \frac{2}{7} \cos 3\theta\right) \tag{9}$$

$$E_b = E_e + E_p - E_0 = \frac{2}{\sqrt{\pi}}\alpha\hbar\omega_{LO} \left(\frac{\lambda}{\omega_{LO}}\right)^{\frac{1}{2}} + V_0 - \frac{\hbar V_0}{4m\lambda R^2} - \frac{\hbar\omega_0^2}{\lambda} \left(1 + \frac{2}{7} \cos 3\theta\right) - \frac{\hbar\omega_c^2}{8\lambda} \tag{10}$$

where E_0 is the strongly coupled polaron's ground-state energy and where E_p and E_e are the independent energies of the phonon and electron, respectively. The LO-phonon mean number was stated as

$$N = \langle \psi_0 | U_2^{-1} \sum_q a_q^\dagger a_q U_2 | \psi_0 \rangle = \alpha \sqrt{\frac{\lambda}{\pi\omega_{LO}}} \tag{11}$$

3. The Effect of Temperature

The electron's properties were calculated as the statistical mean of its various states under finite temperature conditions. Based on the quantum statistical theory (QST) [44], the statistical average of the bulk LO phonons was determined as

$$\bar{N} = \left[\exp\left(\frac{\hbar\omega_{LO}}{K_B T}\right) - 1 \right]^{-1} \quad (12)$$

where K_B is the Boltzmann constant and T is the temperature. The relationship of the VF λ and the temperature T was determined based on self-consistent calculations using Equations (11) and (12). From Equations (8)–(10), the polaron VF, GSE and GSBE were found to be dependent on the temperature T and λ .

4. Results and Discussion

To discuss the theoretical findings in more detail, a RbCl crystal triangular confinement potential QW was adopted to calculate the GSE E_0 , GSBE E_b , VF λ and LO-phonon mean number N . The experiment parameters adapted in the calculations are summarized in Table 1 as they were demonstrated in earlier research [45–47]. The GSE, GSBE, VF and LO-phonon mean number as functions of the applied magnetic field, confinement potential range R , height of AGCPQWs V_0 , polar coordinate system's polar angle θ , confinement strength ω_0 , temperature T and magnetic field's cyclotron frequency ω_c are presented in Figures 1–12; the values of the partial physical quantities used in the figures are shown in Table 2.

Table 1. Values of various parameters used in calculations.

Material	m/m_0	Coupling Constants α	$\hbar\omega_{LO}$ (meV)
RbCl	0.432	3.81	21.45

Table 2. Values of partial parameters used in Figures.

Figures 1a, 2a, 3a and 4a	$\omega_0 = 10 \times 10^{13}$ Hz $\omega_c = 10 \times 10^{13}$ Hz $\theta = 0$ rad
Figures 1b, 2b, 3b and 4b	$\omega_0 = 5 \times 10^{13}$ Hz $\omega_c = 5 \times 10^{13}$ Hz $\theta = 0$ rad
Figures 5a, 6a, 7a and 8a	$\omega_0 = 5 \times 10^{13}$ Hz $\omega_c = 10 \times 10^{13}$ Hz $R = 0.4$ nm
Figures 5b, 6b, 7b and 8b	$\omega_c = 10 \times 10^{13}$ Hz $\theta = 0$ rad $R = 0.4$ nm
Figures 9a, 10a, 11a and 12a	$\omega_0 = 1 \times 10^{13}$ Hz $\omega_c = 1 \times 10^{13}$ Hz $\theta = 0$ rad $R = 1$ nm
Figures 9b, 10b, 11b and 12b	$\omega_0 = 10 \times 10^{13}$ Hz $\theta = 0$ rad $R = 1$ nm

Figures 1–4 show the relationship between the GSE, GSBE, VF, LO-phonon mean number and the influence of the AGCP, respectively. As can be seen from Figure 1, the GSE increased with an increase in the barrier height and a decrease in the range of the AGCPQWs. The reason for this phenomenon was that the AGCP increased with an increase in the barrier height, whereas it decreased with an increase in the range. With an increase in the confinement potential, the confinement strength of the electrons increased in the growth direction of the QW, which promoted the formation of polarons and led to an increase in the GSE. Figure 2 denotes that the GSBE increased with an increase in the barrier height and a decrease in the range of the AGCPQWs. The reason for this phenomenon was the same as that for the effect of the AGCP on the GSE. From Figure 3, we noticed that the VF increased with an increase in the barrier height and a decrease in the range of the AGCPQWs. The reason for this phenomenon was the same as that for the effect of the AGCP on the GSE. This occurred while the movement of the electrons was restricted by the confinement potential in the z direction. Due to a smaller range in the particle motion, the thermal motion energy of the electrons and the interaction between the electron and the phonons, which used the phonons as a medium, increased with an increase in the confinement strength. The VF, thus, rose. These were the results from the intriguing quantum size confinement effects.

Figure 4 describes that the GSBE increased with an increase in the barrier height and a decrease in the range of the AGCPQWs. The intriguing phenomenon in the figure was caused by a stronger coupling of phonons to polarons, which was brought on by an increase in the AGCP. This was compared with the following references: Xiao et al. [48] performed a theoretical investigation on the GSE, GSBE, VF and LO-phonon averages of strongly coupled magnetopolarons in asymmetric semi-exponential quantum wells. Sun et al. [49] performed a theoretical investigation on the effects of the barrier height and range on the vibration frequency, first excited state energy, excitation energy and coherence time in semi-exponential confinement potential QWs. Miao et al. [50] investigated the effect of the anisotropic parabolic confinement potential on the strongly coupled polaron ground state and phonon mean number of RbCl asymmetrical semi-exponential quantum wells. However, this paper attempted to study a TCPQW, and it proved in the experiment that the triangular confinement potential was more than capable of binding electrons, which led to positive energy and stronger polaron motion. The energy was positive, mainly due to the difference in the potential added in the x - y direction.

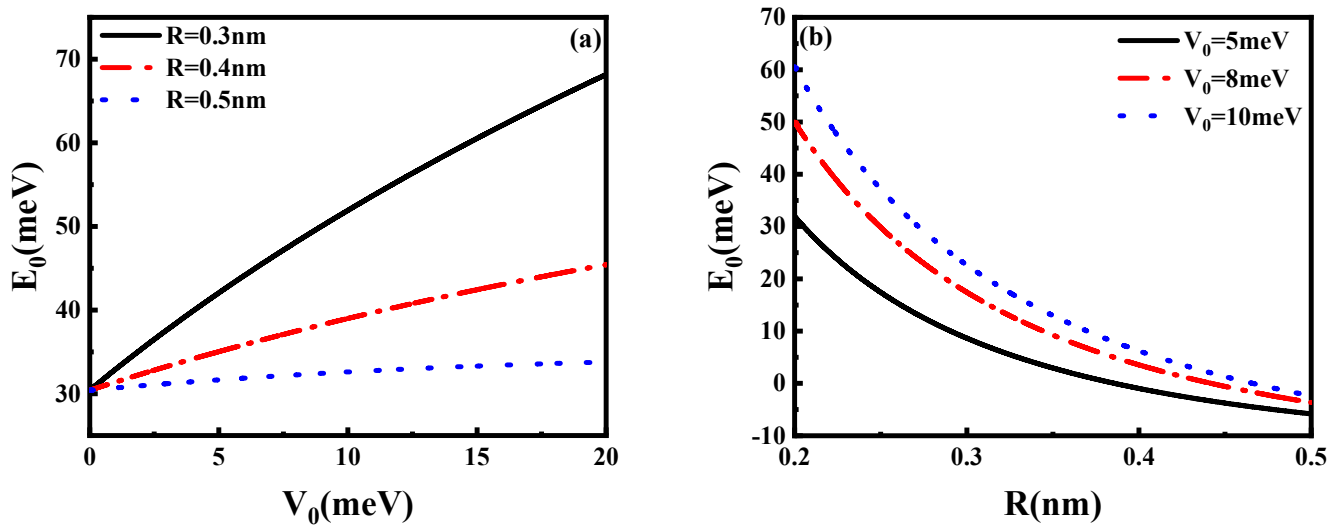


Figure 1. Ground-state energy E_0 versus (a) AGCP barrier height V_0 and (b) AGCP range R .

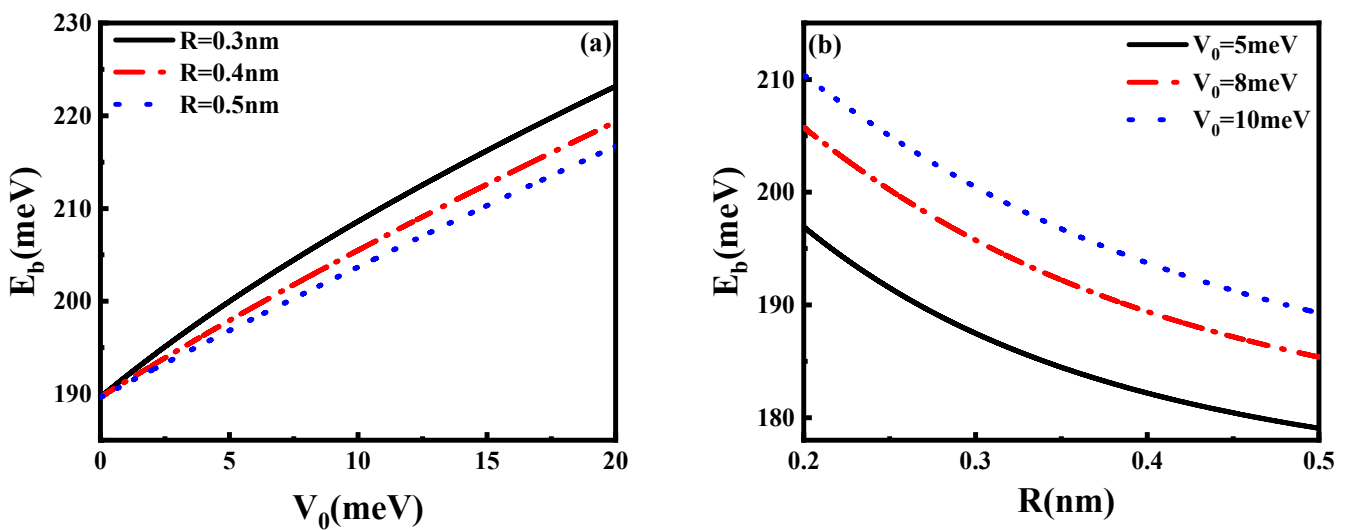


Figure 2. Ground-state binding energy E_b versus (a) AGCP barrier height V_0 and (b) AGCP range R .

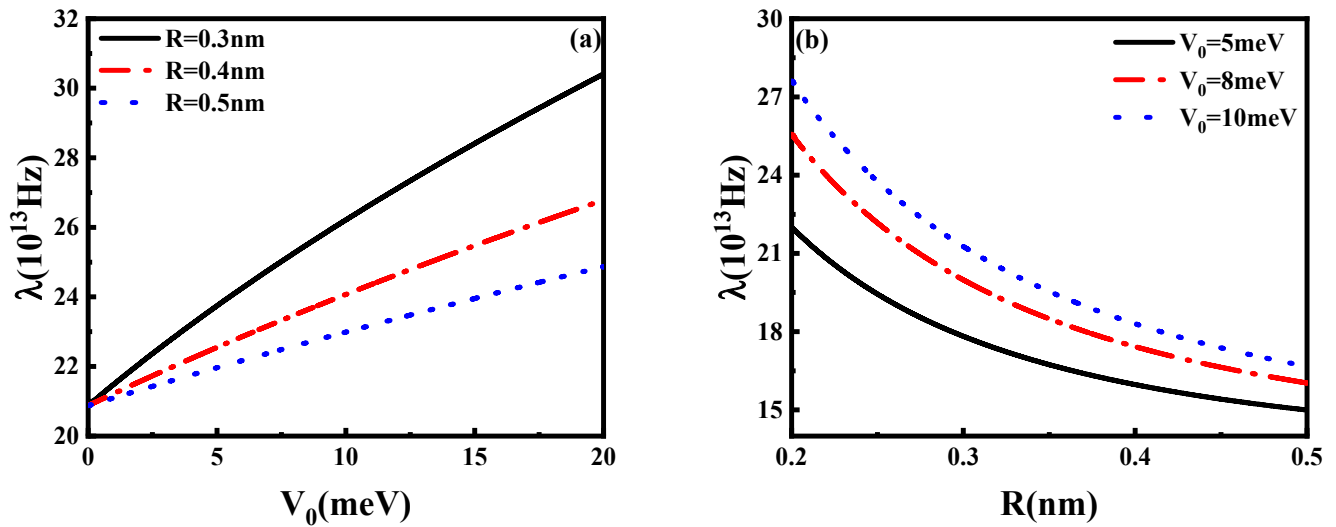


Figure 3. Vibrational frequency λ versus (a) AGCP barrier height V_0 and (b) AGCP range R .

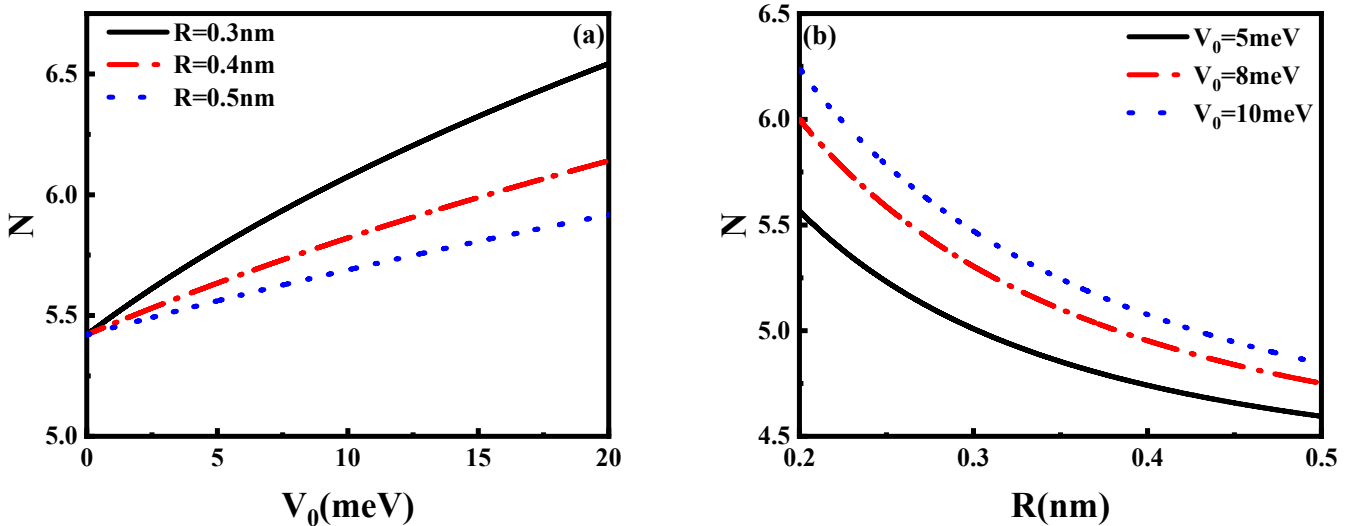


Figure 4. LO-phonon mean number N versus (a) AGCP barrier height V_0 and (b) AGCP range R .

The relation curves of the polar angle and confined strength versus the GSE, GSBE, VF and LO-phonon mean number of strongly coupled magnetopolarons in RbCl TCPQWs of a polar coordinate system are depicted in Figures 5–8. As can be seen in Figure 5a, the absolute value of the GSE of strongly coupled magnetopolarons changed periodically with the polar angle, which was because the TCPQWs formed by the RbCl crystals rotated periodically. It can be observed from Figure 5b that the GSE of strongly coupled magnetopolarons also increased with an increase in the confined strength of the polar coordinate system. This was due to the motion of the electrons being constrained by the limited potential of the polar coordinate system, which, in turn, led to electron–phonon interaction coupling. The range in the particle motion decreased with an increase in the confined intensity so that the energy of the electron–phonon interaction and the electron thermal motion in an acoustic medium could be determined. It is well known that the constrained potential of a polar coordinate system, that is, the triangular confined potential, is a parabolic confined potential which is closest to the real confined potential of a crystal in quantum dots, quantum wires and quantum wells. Compared with the simple parabolic potential, the triangular potential is closer to reality. It can be clearly seen from Figure 6 that the absolute value of the GSBE of strongly coupled magnetopolarons changed periodically with the polar angle and increased with an increase in the limiting potential of the polar coordinate system. The reason for this

phenomenon was consistent with that for the effect of the TCP on the GSE. It is obvious from Figure 7 that the absolute value of the VF of strongly coupled magnetopolarons changed periodically with the polar angle. Moreover, it was enhanced with an increase in the polar coordinate system’s confinement potential. The reason for this phenomenon was the same as that for the effect of the TCP on the GSE. As can be observed in Figure 8, the LO-phonon mean number of strongly coupled magnetopolarons changed periodically with the polar angle and was enhanced with an increase in the polar coordinate system’s confinement potential. The reason for this phenomenon was the same as that for the effect of the TCP on the GSE.

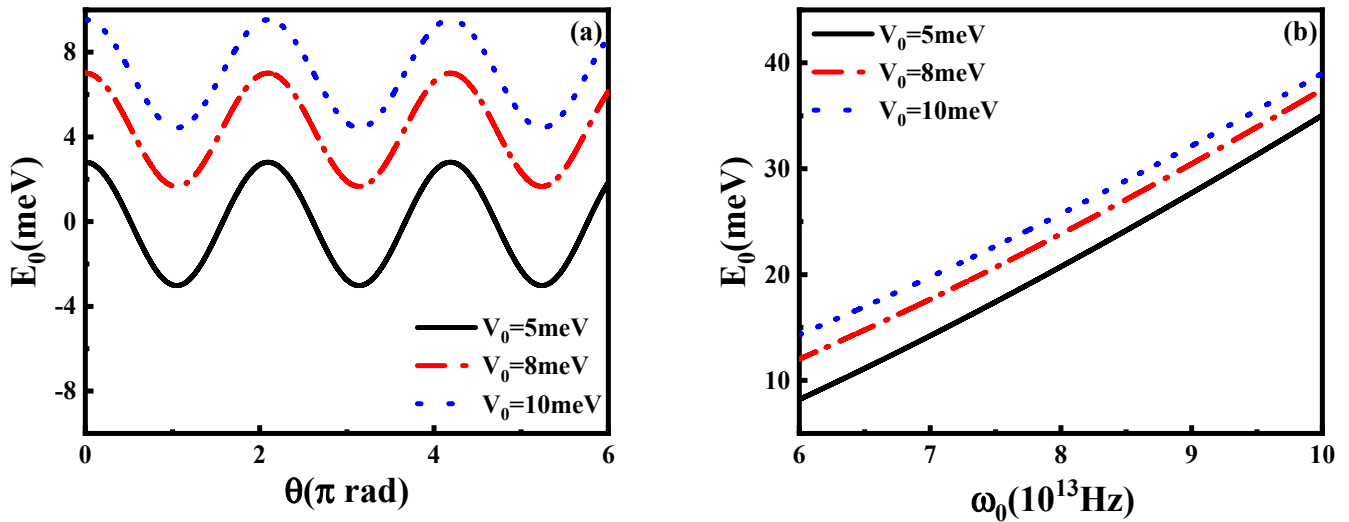


Figure 5. Ground-state energy E_0 versus (a) polar angle θ and (b) confinement strength ω_0 of a polar coordinate system.

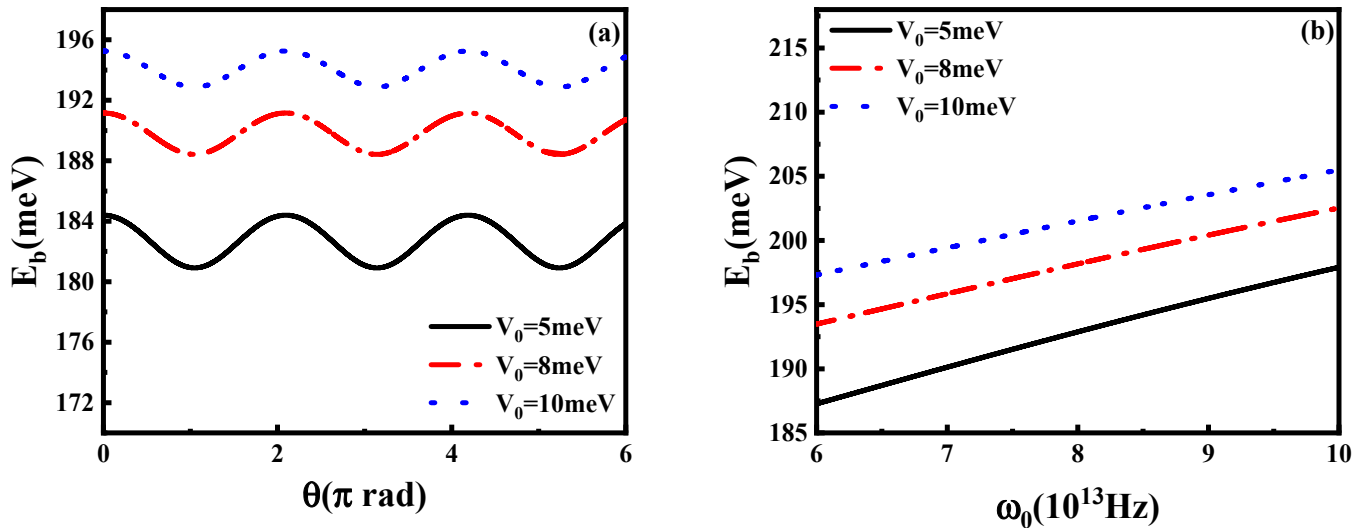


Figure 6. Ground-state binding energy E_b versus (a) polar angle θ and (b) confinement strength ω_0 of a polar coordinate system.

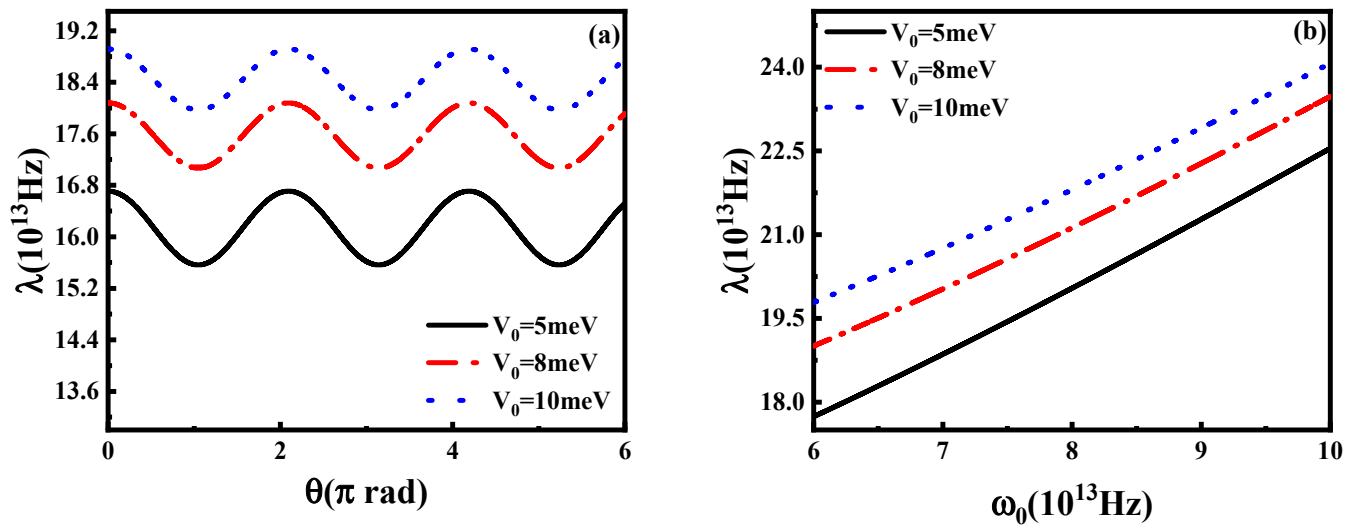


Figure 7. Vibrational frequency λ versus (a) polar angle θ and (b) confinement strength ω_0 of a polar coordinate system.

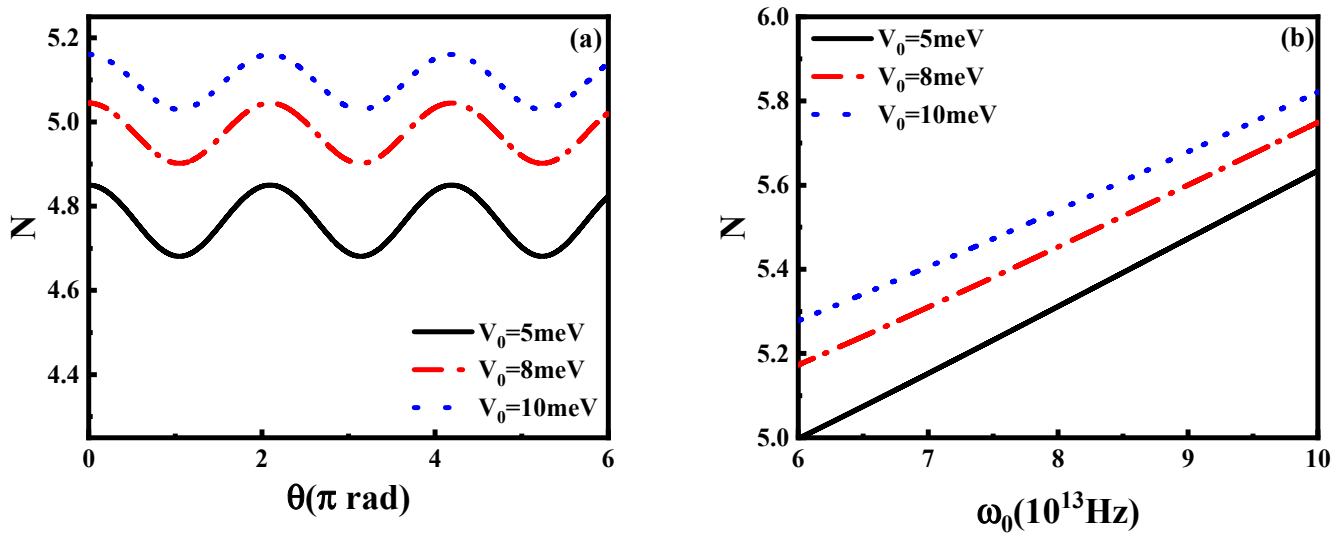


Figure 8. LO-phonon mean number N versus (a) polar angle θ and (b) confinement strength ω_0 of a polar coordinate system.

Figures 9–12 describe the relationship between the GSE, GSBE, VF, LO-phonon mean number and the influence of the magnetic field and temperature, respectively. Moreover, as can be observed in Figure 9, the GSE of the polaron increased with the temperature and cyclotron frequency. The reason for this phenomenon was that the increase in the temperature led to the greater intensification of the thermal movement of the electrons in the polaron and that the application of a magnetic field to the system introduced additional energy to it. However, considering the magnetic field as another confinement for the electrons led to a higher electron wave function overlap. Hence, the electron-phonon interaction was enhanced, which led to the physical quantities being elevated. Figure 10 describes that the GSBE of the polaron increased with the temperature and cyclotron frequency. This occurred because an increase in the temperature resulted in stronger coupling between the electrons and phonons, which, in turn, resulted in an equally strong coupling between the electrons and phonons due to the magnetic field. For this reason, the GSBE of the polaron was enhanced. Figure 11 displays that the VF of the polaron increased with the temperature and cyclotron frequency. This was consistent with the cause of the GBE change. Figure 12 represents that the VF of the polaron increased with the temperature

and cyclotron frequency. The intriguing phenomenon in the figure was caused by stronger coupling of phonons to polarons, which was brought on by the temperature and cyclotron frequency. At a finite temperature, there was an influence of the polaron on the electrons and LO phonons in an external magnetic field, which agreed well with the experimental evidence [51]. In order to investigate the temperature effects on the GSE, GSBE, VF and LO-phonon mean number, the effects are shown in Figures 9a, 10a, 11a and 12a on strongly coupled magnetopolarons in RbCl AGCPQWs in terms of temperature. It was seen that the GSE decreased with an increase in the temperature, and the GSBE, VF and LO-phonon mean number absolute values increased with an increase in the temperature. The reason for this was that, when the system was exposed to heat, extra energy was introduced into the system. Hence, the physical quantities increased. Nonetheless, Figures 10b, 11b and 12b show that the GSE, GSBE, VF and LO-phonon mean number enhanced with an increase in the magnetic field's cyclotron frequency. This was because the application of a magnetic field to the system introduced additional energy to it. However, considering the magnetic field as another confinement of the electrons led to a higher electron wave function overlap. Consequently, the electron-phonon interaction was enhanced, which led to the physical quantities being elevated.

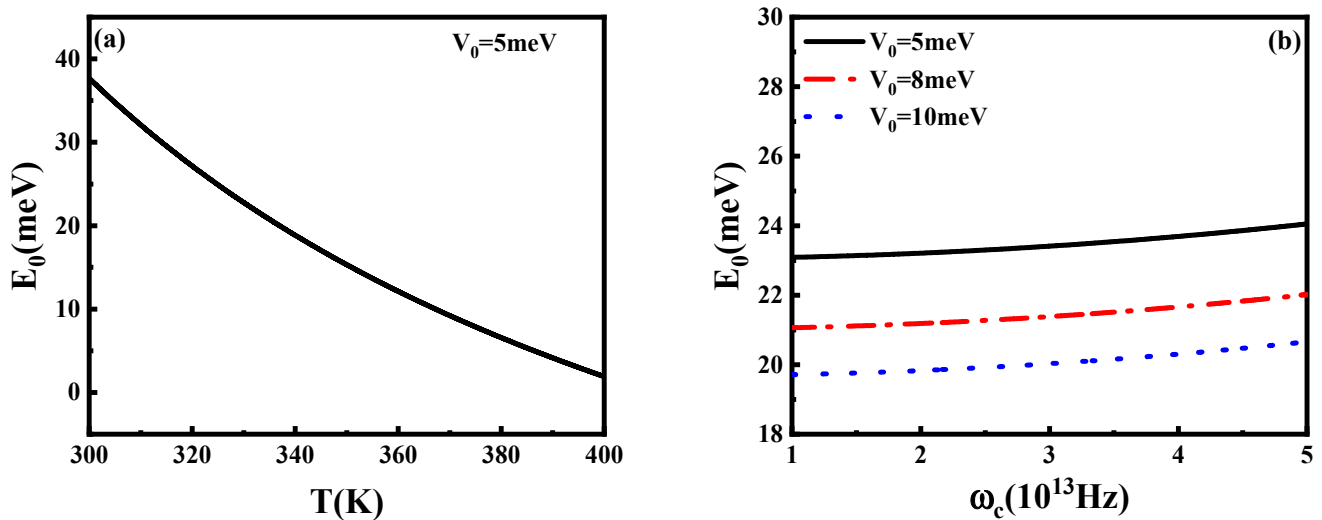


Figure 9. Ground-state energy E_0 (a) versus temperature T and (b) magnetic field's cyclotron frequency ω_c .

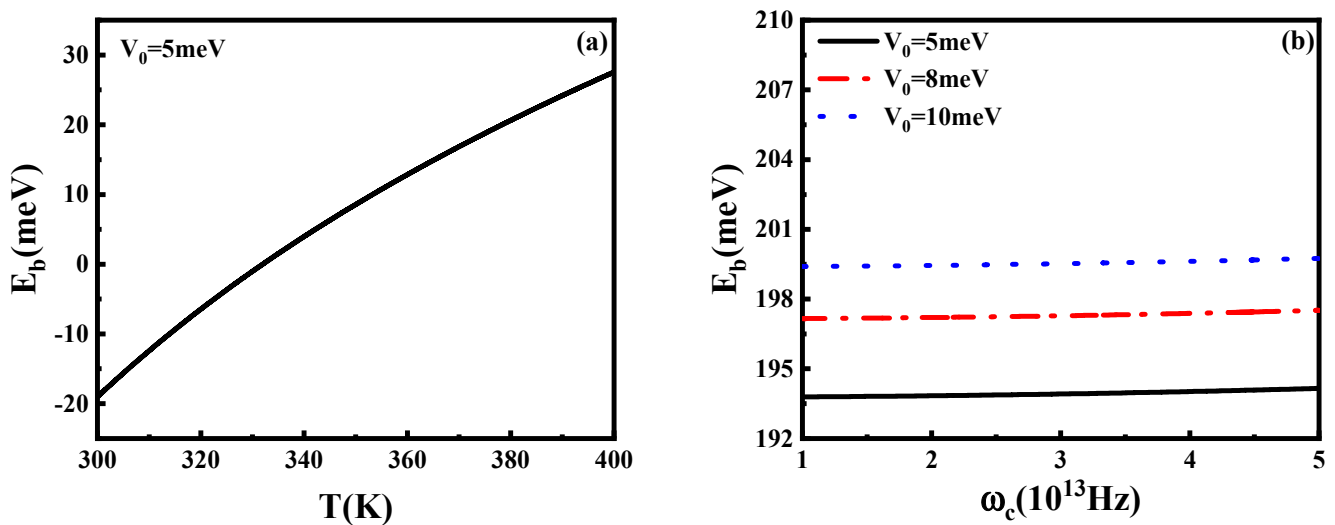


Figure 10. Ground-state binding energy E_b versus (a) temperature T and (b) magnetic field's cyclotron frequency ω_c .

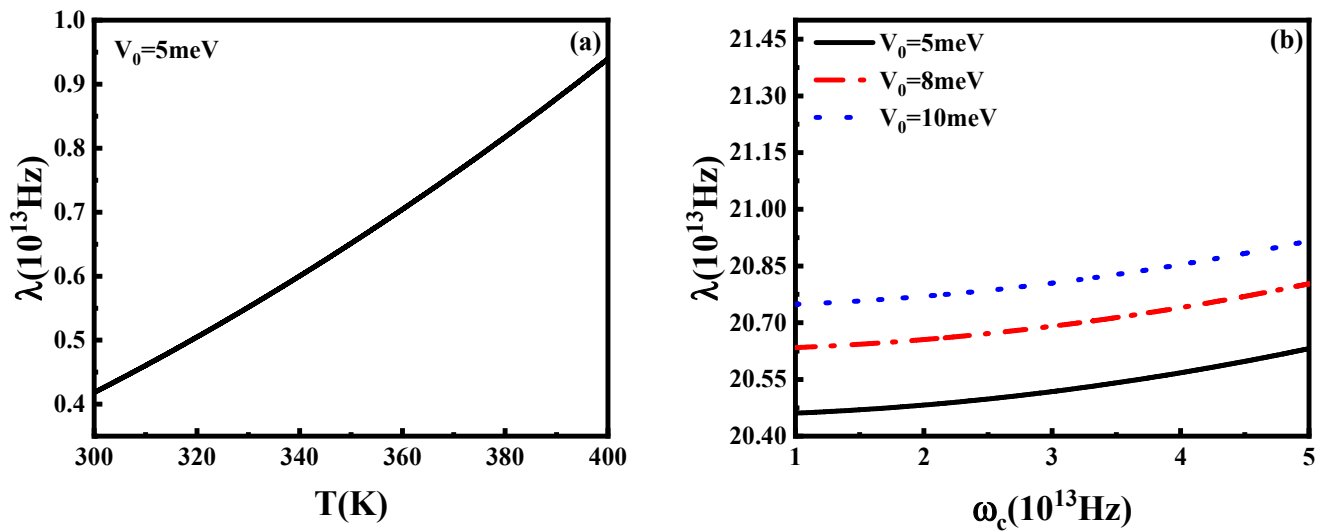


Figure 11. Vibrational frequency λ versus (a) temperature T and (b) magnetic field's cyclotron frequency ω_c .

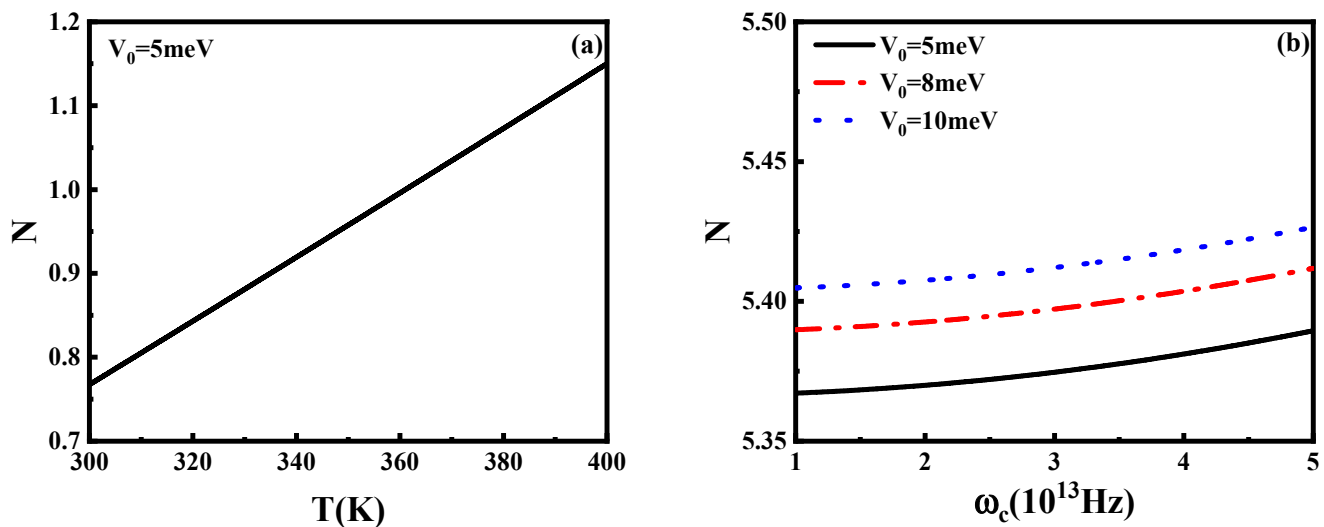


Figure 12. LO-phonon mean number N versus (a) temperature T and (b) magnetic field's cyclotron frequency ω_c .

5. Conclusions

The current electron systems in RbCl AGCPQWs under external magnetic fields were studied. The electronic temperature characteristics of the GSE, GSBE, VF and LO-phonon mean number in strongly coupled magnetopolarons were determined. For this purpose, the GSE, GSBE, VF and LO-phonon mean number were obtained based on the quantum statistics theory, LLP unitary transformation and linear combination operation methods. An expression was derived for the GSE, GSBE, VF and LO-phonon mean number of magnetopolarons as functions of the temperature, AGCP barrier height, AGCP range, magnetic field's cyclotron frequency, polar coordinate system's polar angle and polar coordinate system's confinement strength. According to the obtained results, the average phonon's GSE, GSBE, VF and LO-phonon mean number were decreasing functions of the AGCP range, while they all increased with an increase in the barrier height of the AGCP. The periodic change in the polar angle and the increase in the confined intensity of the polar coordinate systems were also studied. Finally, the changes in the GSE, GSBE, VF and LO-phonon mean number with the temperature and cyclotron frequency were

studied. Not all quantum systems are fully applicable to our theoretical model, but, for the quantum well that was constructed in this paper, the origin of the strange phenomenon of polarons subjected to a triangular confined potential and an asymmetric Gaussian confined potential was theoretically studied, which provided theoretical guidance for further research on polarons.

Author Contributions: Conceptualization, J.G., S.H., X.M., Y.S. and J.X.; methodology, J.G., S.H., X.M., Y.S.; software, J.G., S.H., X.M., Y.S.; validation, X.M., Y.S. and J.X.; formal analysis, J.G., S.H., X.M., Y.S. and J.X.; investigation, J.G., S.H., X.M., Y.S. and J.X.; resources, J.G., S.H., X.M., Y.S. and J.X.; data curation, J.G., S.H., X.M. and Y.S.; writing—original draft preparation, J.G., S.H.; writing—review and editing, J.G., S.H., X.M., Y.S. and J.X.; visualization, X.M., Y.S. and J.X.; supervision, X.M., Y.S. and J.X.; project administration, J.G., S.H., X.M., Y.S. and J.X.; funding acquisition, J.G., S.H., X.M., Y.S. and J.X. All authors have read and agreed to the published version of the manuscript.

Funding: This research was funded by [Scientific Research Projects in Colleges and Universities in Inner Mongolia] grant number [No. NJZY22292], [Natural Science Foundation of Inner Mongolia] grant number [Nos. 2017MS (LH) 0107 and 2022MS01014], [scientific research project of Hulunbuir University] grant number [No. 2022ZKYB09].

Institutional Review Board Statement: Not applicable.

Informed Consent Statement: Not applicable.

Data Availability Statement: Not applicable.

Conflicts of Interest: The authors declare no conflict of interest.

Abbreviations

QW	Quantum Well
AGCP	Asymmetrical Gaussian Confinement Potential
TCPQW	Triangular Confinement Potential Quantum Well
LO	Longitudinal Optical
LLP	Lee–Low–Pines
QST	Quantum Statistical Theory
GSE	Ground-State Energy
GSBE	Ground-State Binding Energy
VF	Vibrational Frequency

References

1. Camacho-Guardian, A.; Bruun, G.M. Landau effective interaction between quasiparticles in a Bose-Einstein condensate. *Phys. Rev. X* **2018**, *8*, 031042. [[CrossRef](#)]
2. Franchini, C.; Reticcioli, M.; Setvin, M.; Diebold, U. Polarons in materials. *Nat. Rev. Mater.* **2021**, *6*, 560–586. [[CrossRef](#)]
3. Emin, D. *Polarons*; Cambridge University Press: Cambridge, UK, 2013.
4. Abolfath, R.M.; Korkusinski, M.; Brabec, T.; Hawrylak, P. Spin textures in strongly coupled electron spin and magnetic or nuclear spin systems in quantum dots. *Phys. Rev. Lett.* **2012**, *108*, 247203. [[CrossRef](#)] [[PubMed](#)]
5. Kaczmarkiewicz, P.; Machnikowski, P. Two-phonon polaron resonances in self-assembled quantum dots. *Phys. Rev. B* **2010**, *81*, 115317. [[CrossRef](#)]
6. Pascual, G.; Boronat, J. Quasiparticle nature of the Bose polaron at finite temperature. *Phys. Rev. Lett.* **2021**, *127*, 205301. [[CrossRef](#)] [[PubMed](#)]
7. Preisler, V.; Ferreira, R.; Hameau, S.; De Vaulchier, L.A.; Guldner, Y.; Sadowski, M.L.; Lemaître, A. Hole–LO phonon interaction in InAs/GaAs quantum dots. *Phys. Rev. B* **2005**, *72*, 115309. [[CrossRef](#)]
8. Piekarczyk, P.; Legut, D.; Baldini, E.; Belvin, C.A.; Kołodziej, T.; Tabiś, W.; Kozłowski, A.; Kakol, Z.; Tarnawski, Z.; Lorenzana, J.; et al. Trimeron-phonon coupling in magnetite. *Phys. Rev. B* **2021**, *103*, 104303. [[CrossRef](#)]
9. Koschorreck, M.; Pertot, D.; Vogt, E.; Fröhlich, B.; Feld, M.; Köhl, M. Attractive and repulsive Fermi polarons in two dimensions. *Nature* **2012**, *485*, 619–622. [[CrossRef](#)]
10. Yamada, Y.; Kanemitsu, Y. Electron-phonon interactions in halide perovskites. *NPG Asia Mater.* **2022**, *14*, 48. [[CrossRef](#)]
11. Lu, N.; Li, L.; Geng, D.; Liu, M. A review for polaron dependent charge transport in organic semiconductor. *Org. Electron.* **2018**, *61*, 223–234. [[CrossRef](#)]
12. Cornelissen, L.J.; Oyanagi, K.; Kikkawa, T.; Qiu, Z.; Kuschel, T.; Bauer, G.E.W.; van Wees, B.J.; Saitoh, E. Nonlocal magnon-polaron transport in yttrium iron garnet. *Phys. Rev. B* **2017**, *96*, 104441. [[CrossRef](#)]

13. Tan, L.B.; Cotlet, O.; Bergschneider, A.; Schmidt, R.; Back, P.; Shimazaki, Y.; Kroner, M.; İmamoğlu, A. Interacting polaron-polaritons. *Phys. Rev. X* **2020**, *10*, 021011. [[CrossRef](#)]
14. Kandemir, B.S.; Cetin, A. Ground-and first-excited state energies of impurity magnetopolaron in an anisotropic quantum dot. *Phys. Rev. B* **2002**, *65*, 054303. [[CrossRef](#)]
15. Ideue, T.; Hamamoto, K.; Koshikawa, S.; Ezawa, M.; Shimizu, S.; Kaneko, Y.; Tokura, Y.; Nagaosa, N.; Iwasa, Y. Bulk rectification effect in a polar semiconductor. *Nat. Phys.* **2017**, *13*, 578–583. [[CrossRef](#)]
16. Wang, Z.; Reimann, K.; Woerner, M.; Elsaesser, T.; Hofstetter, D.; Hwang, J.; Schaff, W.J.; Eastman, L.F. Optical phonon sidebands of electronic intersubband absorption in strongly polar semiconductor heterostructures. *Phys. Rev. Lett.* **2005**, *94*, 037403. [[CrossRef](#)]
17. Beljonne, D.; Cornil, J.; Sirringhaus, H.; Brown, P.J.; Shkunov, M.; Friend, R.H.; Brédas, J.L. Optical signature of delocalized polarons in conjugated polymers. *Adv. Funct. Mater.* **2001**, *11*, 229–234. [[CrossRef](#)]
18. Hu, M.G.; Van de Graaff, M.J.; Kedar, D.; Corson, J.P.; Cornell, E.A.; Jin, D.S. Bose polarons in the strongly interacting regime. *Phys. Rev. Lett.* **2016**, *117*, 055301. [[CrossRef](#)]
19. Yoshida, S.M.; Endo, S.; Levinsen, J.; Parish, M.M. Universality of an impurity in a Bose-Einstein condensate. *Phys. Rev. X* **2018**, *8*, 011024. [[CrossRef](#)]
20. De Teresa, J.M.; Ibarra, M.R.; Algarabel, P.A.; Ritter, C.; Marquina, C.; Blasco, J.; García, J.; Moral, A.; Arnold, Z. Evidence for magnetic polarons in the magnetoresistive perovskites. *Nature* **1997**, *386*, 256–259. [[CrossRef](#)]
21. Zheng, F.; Wang, L. Large polaron formation and its effect on electron transport in hybrid perovskites. *Energy Environ. Sci.* **2019**, *12*, 1219–1230. [[CrossRef](#)]
22. Sarma, S.D. Theory of two-dimensional magnetopolarons. *Phys. Rev. Lett.* **1984**, *52*, 859. [[CrossRef](#)]
23. Boebinger, G.S.; Levi, A.F.; Schmitt-Rink, S.; Passner, A.; Pfeiffer, L.N.; West, K.W. Direct observation of two-dimensional magnetopolarons in a resonant tunnel junction. *Phys. Rev. Lett.* **1990**, *65*, 235. [[CrossRef](#)]
24. Dietl, T.; Spałek, J. Effect of fluctuations of magnetization on the bound magnetic polaron: Comparison with experiment. *Phys. Rev. Lett.* **1982**, *48*, 355. [[CrossRef](#)]
25. Wu, X.; Peeters, F.M.; Devreese, J.T. Two-dimensional polaron in a magnetic field. *Phys. Rev. B* **1985**, *32*, 7964.
26. Hai, G.Q.; Peeters, F.M. Magnetopolaron effect in parabolic quantum wells in tilted magnetic fields. *Phys. Rev. B* **1999**, *60*, 8984. [[CrossRef](#)]
27. Junior, L.A.R.; Stafström, S. Polaron stability in molecular semiconductors: Theoretical insight into the impact of the temperature, electric field and the system dimensionality. *Phys. Chem. Chem. Phys.* **2015**, *17*, 8973–8982. [[CrossRef](#)]
28. Bonn, M.; Miyata, K.; Hendry, E.; Zhu, X.Y. Role of dielectric drag in polaron mobility in lead halide perovskites. *ACS Energy Lett.* **2017**, *2*, 2555–2562. [[CrossRef](#)]
29. Astrakharchik, G.E.; Ardila, L.A.P.; Schmidt, R.; Jachymski, K.; Negretti, A. Ionic polaron in a Bose-Einstein condensate. *Commun. Phys.* **2021**, *4*, 94. [[CrossRef](#)]
30. Guenther, N.E.; Massignan, P.; Lewenstein, M.; Bruun, G.M. Bose polarons at finite temperature and strong coupling. *Phys. Rev. Lett.* **2018**, *120*, 050405. [[CrossRef](#)]
31. Li, W.S.; Gu, S.W.; Au-Yeung, T.C.; Yeung, Y.Y. Effects of the parabolic potential and confined phonons on the polaron in a quantum wire. *Phys. Rev. B* **1992**, *46*, 4630. [[CrossRef](#)]
32. Shi, J.; Zhu, X.; Liu, Z.; Pan, S.H.; Li, X.Y. Polaron effects in asymmetric semiconductor quantum-well structures. *Phys. Rev. B* **1997**, *55*, 4670. [[CrossRef](#)]
33. Fotue, A.J.; Kenfack, S.C.; Tiotsop, M.; Isofa, N.; Wirngo, A.V.; Djemmo, M.P.T.; Fotsin, H.; Fai, L.C. Shannon entropy and decoherence of bound magnetopolaron in a modified cylindrical quantum dot. *Mod. Phys. Lett. B* **2015**, *29*, 1550241. [[CrossRef](#)]
34. Flebus, B.; Shen, K.; Kikkawa, T.; Uchida, K.; Qiu, Z.Y.; Saitoh, E.; Duine, R.A.; Bauer, G.E.W. Magnon-polaron transport in magnetic insulators. *Phys. Rev. B* **2017**, *95*, 144420. [[CrossRef](#)]
35. Kikkawa, T.; Shen, K.; Flebus, B.; Duine, R.A.; Uchida, K.; Qiu, Z.Y.; Bauer, G.E.W.; Saitoh, E. Magnon polarons in the spin Seebeck effect. *Phys. Rev. Lett.* **2016**, *117*, 207203. [[CrossRef](#)] [[PubMed](#)]
36. Li, J.; Simensen, H.T.; Reitz, D.; Sun, Q.Y.; Yuan, W.; Li, C.; Tserkovnyak, Y.; Brataas, A.; Shi, J. Observation of magnon polarons in a uniaxial antiferromagnetic insulator. *Phys. Rev. Lett.* **2020**, *125*, 217201. [[CrossRef](#)] [[PubMed](#)]
37. Mei, J.H.; Zhang, B.; Xiao, J.L.; Sun, Y.; Zhang, W.; Miao, X.J.; Sarengaowa; Ma, X.J. Effect of double-constrained potential on the ground-state binding energy of magnetopolaron in a quantum well. *Int. J. Mod. Phys. B* **2022**, 2350072. [[CrossRef](#)]
38. Qiu, W.; Sun, Y.; Xiao, J.L. Parabolic Potential Effect on Binding Energy of Impurity Polaron in Asymmetrical Semi-Exponential Quantum Wells. *Iran. J. Sci. Technol. Trans. A Sci.* **2021**, *45*, 2233–2239. [[CrossRef](#)]
39. Zhang, L.; Xie, H.J.; Chen, C.Y. Fröhlich electron-phonon interaction Hamiltonian in a quantum dot quantum well. *Phys. Rev. B* **2002**, *66*, 205326. [[CrossRef](#)]
40. Melnikov, D.V.; Fowler, W.B. Electron-phonon interaction in a spherical quantum dot with finite potential barriers: The Fröhlich Hamiltonian. *Phys. Rev. B* **2001**, *64*, 245320. [[CrossRef](#)]
41. Giustino, F. Electron-phonon interactions from first principles. *Rev. Mod. Phys.* **2017**, *89*, 015003. [[CrossRef](#)]
42. Lee, T.D.; Low, F.E.; Pines, D. The motion of slow electrons in a polar crystal. *Phys. Rev.* **1953**, *90*, 297. [[CrossRef](#)]
43. Huybrechts, W.J. Internal excited state of the optical polaron. *J. Phys. C Solid State Phys.* **1977**, *10*, 3761. [[CrossRef](#)]
44. Whitfield, G.; Engineer, M. Temperature dependence of the polaron. *Phys. Rev. B* **1975**, *12*, 5472. [[CrossRef](#)]

45. Schilcher, M.J.; Robinson, P.J.; Abramovitch, D.J.; Tan, L.Z.; Rappe, A.M.; Reichman, D.R.; Egger, D.A. The significance of polarons and dynamic disorder in halide perovskites. *ACS Energy Lett.* **2021**, *6*, 2162–2173. [[CrossRef](#)]
46. Zou, S.; Kamran, M.A.; Shi, L.J.; Liu, R.; Guo, S.; Kavokin, A.; Zou, B. Bosonic lasing from collective exciton magnetic polarons in diluted magnetic nanowires and nanobelts. *ACS Photonics* **2016**, *3*, 1809–1817. [[CrossRef](#)]
47. Hackens, B.; Faniel, S.; Gustin, C.; Wallart, X.; Bollaert, S.; Cappy, A.; Bayot, V. Dwell-time-limited coherence in open quantum dots. *Phys. Rev. Lett.* **2005**, *94*, 146802. [[CrossRef](#)] [[PubMed](#)]
48. Xiao, W.; Miao, X.J.; Sun, Y.; Ma, X.J.; Xiao, J.L. Parabolic Potential and Temperature Effects on the Magnetopolaron in a RbCl Asymmetrical Semi-exponential Quantum Well. *J. Low Temp. Phys.* **2022**, 1–23. [[CrossRef](#)]
49. Sun, Y.; Xiao, J.L. Coherence effects of the strongly-coupled optical polaron-level qubit in a quantum well with asymmetrical semi-exponential potential. *Superlattices Microstruct.* **2020**, *145*, 106617. [[CrossRef](#)]
50. Miao, X.J.; Sun, Y.; Xiao, J.L. Anisotropic parabolic confinement potential effect on polaron ground state and phonon's number in the RbCl asymmetrical quantum wells. *Indian J. Phys.* **2022**, *96*, 1969–1973. [[CrossRef](#)]
51. Jo, I.; Hsu, I.K.; Lee, Y.J.; Sadeghi, M.M.; Kim, S.; Cronin, S.; Tutuc, E.; Banerjee, S.K.; Yao, Z.; Shi, L. Low-frequency acoustic phonon temperature distribution in electrically biased graphene. *Nano Lett.* **2011**, *11*, 85–90. [[CrossRef](#)]